Determination of Number Density and Velocity of Sputtered Particles by Cavity Ring-Down Spectroscopy

IEPC-2005-300

Presented at the 29th International Electric Propulsion Conference, Princeton University, October 31 – November 4, 2005

Azer P. Yalin*, Vijaya Surla†
Colorado State University, Fort Collins, Colorado, 80523

Abstract: Sputter erosion is a critically important process in many electric propulsion (EP) devices, from the point of view of both lifetime assessment and contamination assessment. We report the use of cavity ring-down spectroscopy (CRDS) as a diagnostic tool to quantify sputter erosion. We discuss measurements of sputtered particle number density and velocity obtained from a bench-top setup consisting of an ion beam incident on a planar target. The number density measurements are validated by comparison with a simple sputter model. The detection limits of our CRDS system are found to be very adequate for studies of EP devices. The CRDS velocity measurements are obtained by a Doppler shift method and are validated by comparison with sputter simulations. We also present CRDS studies of excited state population distributions and velocities of sputtered particles and discuss the measured distributions. In summary, we find that the CRDS technique provides a sensitive and versatile tool for sputter erosion studies for EP applications.

Nomenclature

$A(\nu)$	=	Absorption lineshape, Hz^{-1}
A_{ki}	=	Einstein *A* coefficient, 1/s
Abs_{Eff}	=	Effective absorbance
c	=	Speed of light, 2.998 x 10^8 m/s
E_b	=	Binding energy, eV
g_i	=	Degeneracy of state *i*
I_{sp}	=	Specific impulse, s
$k(\nu)$	=	Absorption coefficient, m^{-1}
$k_{eff}(\nu)$	=	Effective absorption coefficient, m^{-1}
$L(\nu)$	=	Laser lineshape, Hz^{-1}
l	=	Length of the ring-down cavity, m
M	=	Molar mass, g
N_i	=	Lower state concentration, m^{-3}
$n(\vec{V})$	=	Velocity distribution, m^{-3} $(m/s)^{-1}$
R	=	Mirror reflectivity
ROC	=	Mirror radius-of-curvature, m
$S(t,\nu)$	=	Ring-down signal
$S(\nu)$	=	Doppler shifted lineshape, Hz^{-1}
$S'(\nu)$	=	Measured lineshape, Hz^{-1}
T_B	=	Boltzmann temperature, K
$\vec{V}$	=	Velocity vector, m/s
V_0	=	Component of V parallel to optical axis
V_b	=	Velocity associated with E_b, m/s
$y(\alpha)$	=	Differential sputter yield, sr^{-1}
ν	=	Laser frequency, Hz
ν_{ki}	=	Transition frequency, 1/s
τ	=	Ring-down time, s
τ_0	=	Empty cavity ring-down time, s
θ	=	Angle between $\vec{V}$ and optical axis
$\Delta\lambda$	=	Doppler shift in wavelength, m
$\Delta\nu$	=	Doppler shift in frequency, Hz
$\delta(\nu)$	=	Delta function

I. Introduction

The lifetimes of many electric propulsion (EP) devices are fundamentally limited by sputter erosion of certain critical components including guard rings, ion optics, and electrodes. The combination of EP system

* Assistant Professor, Mechanical Engineering, ayalin@engr.colostate.edu.
† Graduate Student, Mechanical Engineering, vijay.surla@colostate.edu.

capabilities and past successes are leading toward more ambitious missions requiring much greater thruster lifetimes. With proposed thrust durations now as long as 5-10+ years, ground-based life tests are becoming increasingly impractical. Therefore, lifetime assessments are increasingly relying on numerical modeling approaches. Clearly, such models require basic sputtering data (e.g. differential sputter yields for the ions and materials of interest) to yield accurate results. Further, the fidelity of such models should be tested against experimental studies. To address both these needs, there arises a need for sensitive sputtering diagnostics. A related EP concern, associated with sputtering, is the problem of spacecraft contamination by sputtered particles that condense on spacecraft surfaces. The state-of-the-art is to use numerical models to track the sputter products and to estimate the extent of such contamination problems. Again, these codes require fundamental sputtering data both as inputs and for validation. In this work, we provide an overview of the use of cavity ring-down spectroscopy (CRDS) as a sputter diagnostic in support of EP lifetime and contamination assessments.

A number of sputtering diagnostic methods exist, and CRDS may be viewed as an extension or complement to these methods. There are a host of non-optical techniques that may be used for sputter erosion measurements including optical-profilometry and weight-loss and weight-deposition techniques. In some cases these techniques provide useful information, but often they suffer from lack of sensitivity (owing to the low erosion rates of interest – typically ~0.1-10 μm/hr) and in some cases systematic biases (e.g. ion implantation leads to error in weight loss measurements, and unknown sticking coefficients can complicate weight deposition measurements). In terms of EP applications, the best available means to measure thruster wear in real time is the surface layer activation (SLA) technique, in which some of the eroding surface of the thruster is made radioactive. The degree of remaining radioactivity is recorded as a function of time, and yields the erosion rate[1]. The SLA technique is sensitive and accurate, but tends to be time consuming and costly. Successful use of these non-optical approaches allows determination of the erosion rate; however, with the exception of deposition approaches, does not generally yield information on the fate of the sputtered particles (critical for contamination assessments) nor species-specific information (useful for contamination assessments of multi-component materials). Optical techniques provide the possibility of species-specific measurements and in some cases enhanced sensitivity. Laser induced fluorescence (LIF) has been used in a number of studies[2, 3] and has proven invaluable for measuring the velocity (energy) profiles of sputtered particles. However, LIF has serious limitations for quantitative number density measurements (needed for determination of sputter yield and erosion rate). CRDS is much better suited to measurements of species number density owing to its directly quantitative nature. Its spectroscopic nature allows species-specific information as well as velocity (energy) information through Doppler shifts. Furthermore, its very high-sensitivity makes it amenable to rapid (near real time) sputtering measurements, and thus affords the possibility of performing *in situ* device studies where erosion is recorded as a function of the device set point. A drawback of the CRDS technique (common to all laser absorption methods) is its path-integrated nature.

In section II of this paper we review the theory of cavity ring-down spectroscopy. In Section III we present the design of the bench-top CRDS/sputtering system used for diagnostic development. Results of number density measurements of several sputtered species, including comparison with a simple sputter model are presented in Section IV. Sections V and VI discuss velocity measurements as well as studies of the distribution of excited electron states of sputtered particles (including "anomalous" non-Boltzmann behavior). Finally, the work is summarized, and future directions are discussed in Section 7.

II. Cavity Ring-Down Spectroscopy (CRDS)

CRDS is a highly sensitive laser-based absorption technique[4,5] that is directly quantifiable and thus well suited to measurements of low concentrations of sputtered particles. It is an absorption technique, so that unlike fluorescence and emission measurements, ground states are measurable and there are no quenching interferences. Measuring ground states is advantageous since these levels typically contain a large fraction of the overall species population. Thus, the signals tend to be larger and can be accurately related to the desired overall species population. As shown in Fig. 1, the basic idea is to house the absorbing sample (i.e. the sputtered atoms) within a high-finesse optical cavity formed from high-reflectivity mirrors (R~0.9999). The interrogating laser beam is coupled into the optical cavity where it "bounces" many times back-and-forth between the mirrors. Owing to the high reflectivity, the light within the cavity makes many passes (e.g. ~10^4 passes for R~0.9999) within the cavity, and the effective path length and thus sensitivity is greatly increased. A detector placed behind the cavity measures the temporal decay of optical intensity within the cavity. The difference in the temporal decay rate with and without the absorber (or with the laser tuned on/off the resonance) yields the sample concentration. The technique has been used widely for the

measurements of trace species in flames, plasmas, and the atmosphere, and we have recently pioneered its use for sputter measurements for electric propulsion applications[6-8].

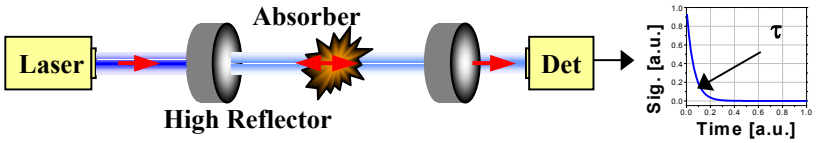

Figure 1. Schematic diagram of cavity ring-down spectroscopy (CRDS). Laser light is coupled into a high reflectivity cavity where it bounces back and forth many times. A detector behind the cavity measures the decay of the light intensity inside the cavity, which may be related to the concentration of the absorbing species.

The technique affords high sensitivity owing to a combination of long effective path length and insensitivity to laser energy fluctuations (since a rate is measured). Under appropriate conditions, the ring-down signal $S(t, \nu)$ decays single exponentially[9,10] versus time as:

$$S(t,\nu) = S_0 \exp\left[-t/\tau(\nu)\right]$$
$$1/\tau(\nu) = \frac{c}{l}\left[\int k_{Eff}(x,\nu)dx + (1-R)\right] \quad ; \quad k_{Eff}(\nu) \equiv \int_{-\infty}^{+\infty} d\nu'\, L(\nu'-\nu)\, k(\nu') \tag{1}$$

where τ is the 1/e time of the decay (termed the ring-down time), c is the speed of light, l is the cavity length, $k_{Eff}(\nu)$ is the effective absorption coefficient, ν is the laser frequency, $1-R$ is the effective mirror loss (including scattering and all cavity losses), $L(\nu)$ is the laser lineshape function, and $k(\nu)$ absorption coefficient. If the absorber is uniformly present over a column length l_{abs}, then $\int k_{eff}(x,\nu)dx$ can be replaced with the product $k_{Eff}(\nu)l_{abs}$. As in conventional absorption, the effective absorption coefficient accounts for line broadening arising from the laser lineshape. In practice, the measured ring-down signal is fitted with an exponential, and the ring-down time τ is extracted. Combining τ with the "empty cavity ring-down time", τ_0 (which in practice is measured by detuning the laser) allows determination of the (effective) sample absorbance, Abs_{Eff}, and (effective) absorption coefficient, k_{Eff}:

$$Abs_{Eff}(\nu) \equiv l_{abs}k_{Eff}(\nu) = \frac{l}{c}\left[\frac{1}{\tau(\nu)} - \frac{1}{\tau_0}\right] \tag{2}$$

As in conventional absorption, both the laser and absorber lineshapes are needed to determine the actual absorbance (and number density) if the absorption is measured at a single wavelength. A more practical approach is to scan the laser frequency across the absorption line and to measure the frequency-integrated spectrum (i.e. the line area). Because the area of the effective absorbance spectrum is equivalent to the area of the (actual) absorbance spectrum, this method removes lineshape dependences. Assuming the absorption line parameters are known, the measured area $\int Abs_{eff}(\nu)d\nu$ of a transition from lower state i to upper state k can be readily converted to the path-integrated concentration of the lower state $\int N_i dx$ as:

$$\int N_i dx = 8\pi \frac{g_i}{g_k}\frac{\nu_{ki}^2}{A_{ki}c^2}\left(\int Abs_{Eff}(\nu)\,d\nu\right) \tag{3}$$

where g_i, g_k are the level degeneracies, ν_{ki} is the transition frequency, A_{ki} is the transition Einstein A coefficient, and c is the speed of light. Actual concentration can be determined from the path-integrated concentration in several ways: assume a uniform concentration profile over a known column length, l_{abs}, as is done in this work; perform scans at different chords and use an Abel inversion for axisymetric cases; or use an assumed profile shape (with amplitude scaled by the experimental path-integrated value). We have recently demonstrated the use of CRDS to extract velocity information from the measured spectral lineshapes[8]. The approach is based upon Doppler shifts due to velocity components along the optical axis and will be described in Section V.

III. Bench-Top Measurement Set-Up

Fig. 2 shows a schematic diagram of the bench-top sputtering apparatus employed for CRDS diagnostic development[6,7]. The apparatus allows us to use CRDS to probe sputtered particles created by an ion beam incident upon a target. The key components are an ion beam and target, housed within a vacuum facility. A roughing and turbo-pump (Turbo-V550) are used to bring the pressure to approximately 10^{-6} torr under no-flow conditions. A small argon flow (1 sccm) is used to feed the system. In the current experiments, the target is typically a disc of diameter 8 cm. The ion beam is extracted from an 8-cm diameter structurally integrated thruster [11] obtained from NASA, and modified to operate on an inert gas, and to use refractory metal filaments for both the main and neutralizer cathodes in place of the hollow cathodes used in the original design. In these experiments, the beam is normally incident upon the target. The thruster operates with an IonTech power supply (MPS 3000), with typical beam currents and voltages of about 10-100 mA, and 400-1000 V respectively. We typically mask the ion beam so that it has an active area of 8 cm x 2.5 cm (with the 8 cm extent oriented parallel to the optical axis).

Past research shows that sputter yields from metallic species (as well as the velocities of the sputtered particles) can be effected by oxygen and other impurities[3]. Because we operate at relatively high current densities (approximately 1 mA/cm^2), we compute that the flux of ions to the target is at least an order of magnitude higher than the flux of impurity particles, so that poisoning effects should be negligible. We have verified this conclusion experimentally by varying the chamber pressure (and impurity level) during sputtering measurements, and finding no appreciable effect on the sputtering data.

The CRDS set-up, schematically shown in Fig.3, uses a broadly tunable optical parametric oscillator (OPO) laser system (doubled idler) as the light source to probe optical transitions in the ~370-400 nm region. Laser parameters are: repetition rate = 10 Hz, pulse width ~ 7 ns, pulse energy ~ 3 mJ, and linewidth ~0.002 nm. We use a linear ring-down cavity of 75 cm length with 50 cm radius-of-curvature (ROC) mirrors. Modeling results by Spuler et al.[12] indicate that this will be a near optimal cavity geometry in terms of spatial resolution (beam walk) and stability. In order to prevent possible saturation effects, the laser energy is reduced with an attenuator to ~100 μJ/pulse prior to cavity injection. For this input energy level, we have verified that our spectra and number density measurements are unaffected by laser energy. The ring-down signal is collected behind the output mirror with a fast photomultiplier tube (Hamamatsu R3896). Ring-down signals are fit between 90%-10% of the peak amplitude. We use area (frequency-integrated) measurements of absorbance in our analyses. Following the theory of Reference 10 we have used reduced temporal fitting windows to verify that our measurements are not affected by laser bandwidth effects (to within the quoted error bars).

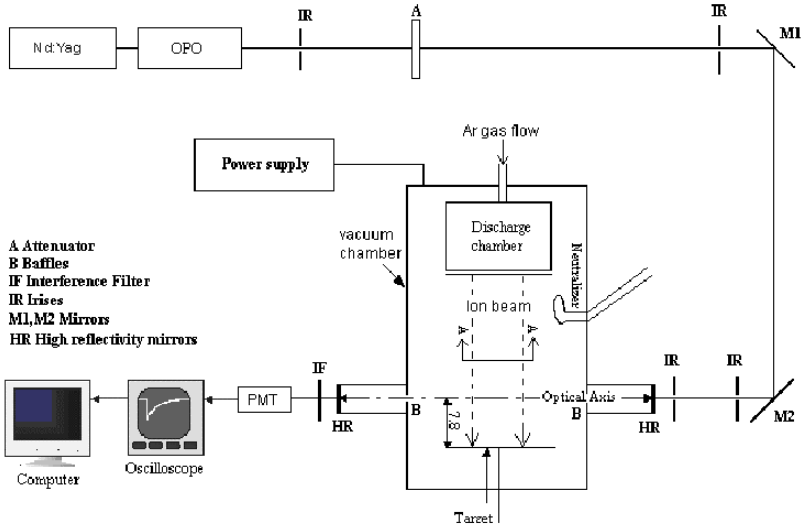

Figure 2. Schematic diagram of sputtering apparatus and CRDS system. The ion beam is normally incident upon the target and optical axis is located 7.8 cm upstream of the target. The ring-down cavity has a length of 0.75 m, and uses 0.5-m radius of curvature mirrors. An OPO laser system is used as the light source, and a photomultiplier tube (PMT) detects the light exiting the cavity.

IV. Number Density Measurements

A. Energy Level Diagrams and Measured Spectra

We discuss number density measurements of four sputtered species: aluminum, iron, titanium, and molybdenum. For each species of interest we have probed several absorption lines (electronic transitions) in the spectral region of ~370-400 nm. Spectroscopic models (including lineshape effects) are used to identify appropriate spectroscopic transitions, and to quantitatively analyze data. The measurements are based on probing absorption lines originating from low-lying levels within the ground state multiplet. The left panels of Fig. 3 show partial energy level diagrams for aluminum, iron, molybdenum, and titanium. For all energy level diagrams in this work, all energy levels below 1 eV are included, wavelengths are given as vacuum, and all parameters (energy configurations, terms, J values, and wavelength) are from NIST[13]. For aluminum, the electronic ground state multiplet has 2 fine structure levels (J=1/2, 3/2), and our absorbance spectrum is based on probing one line from each state. For iron, the ground state multiplet $3d^6 4s^2\ ^5D$ is split into 5 levels (J=4, 3,.., 0). The molybdenum ground state has no fine structure, and our CRDS detection scheme is based on probing lines originating from the (same) ground state energy level (379.93 nm and 386.52 nm). For titanium, the ground state multiplet consists of 3 fine structure levels (J=2, 3, 4) and we measure one line from each level (at 398.29, 399.98, and 395.75 nm respectively).

We have used CRDS to record spectra (from sputtered atoms) of each of these four species. Sputtering is by normally incident argon ions of energy 750 eV and the optical axis is 7.8 cm above the target. Equation (2) is used to convert the measured ring-down signals to (effective) absorbance, while Eq. (3) related the line areas to path-integrated concentration. The right panels of Fig. 3 show plots of variation of species number density versus beam current for each species. In these plots we have assumed a uniform number density over a path length of 8 cm in order to convert the measured path-integrated number density into a representative value of number density. In each case we plot the overall population of the species, i.e. N, not just the population(s) N_i of the specific energy level(s) probed. In order to convert the measured (state-specific) population(s) N_i to the overall population N we assume a Boltzmann distribution (see also Section VI) for the population distribution. The Boltzmann temperature, T_B, is found from a Boltzmann analysis of the measured states, and is assumed to apply over all the states (all multiplets and all fine structure levels) for the given atom. Under this assumption (and for our conditions) we find that for each species studied greater than 98% of the total population resides in the ground state multiplet, so that such a scaling ("correction") should be relatively robust. As discussed in Section VI, there are some "unusual" cases that deviate significantly from Boltzmann statistics, though for the species considered here our studies indicate the assumption is reasonably valid. The insets of the right panels of Fig. 3 show the experimentally measured spectra for each species (for a current of 18 mA for Al, Ti, and Mo, and 20 mA for Fe). The points are experimental measurements while the solid line is a series (sum) of Voigt profiles fitted to the peaks (with a single Voigt used for each absorption feature). Interpretation and validation of the measured number densities is discussed in the following section.

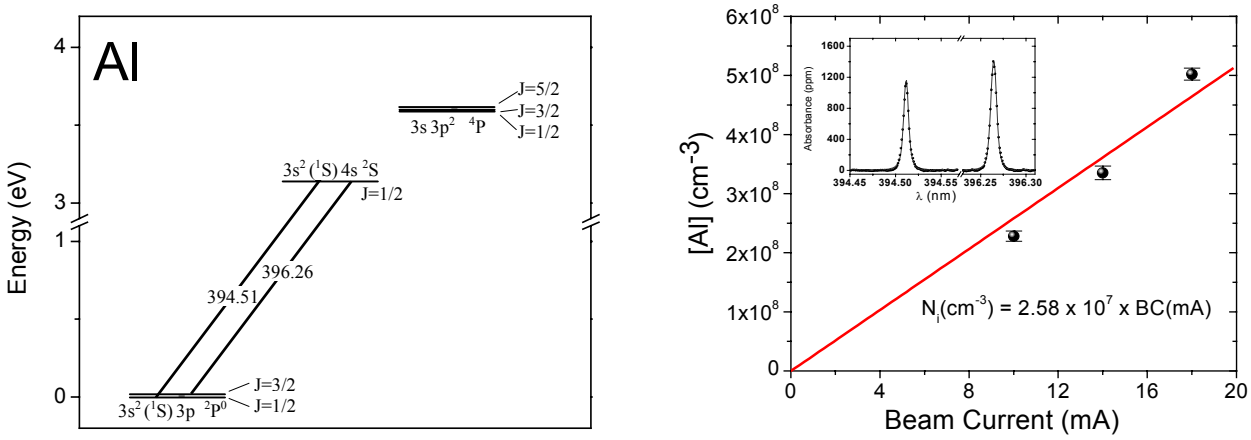

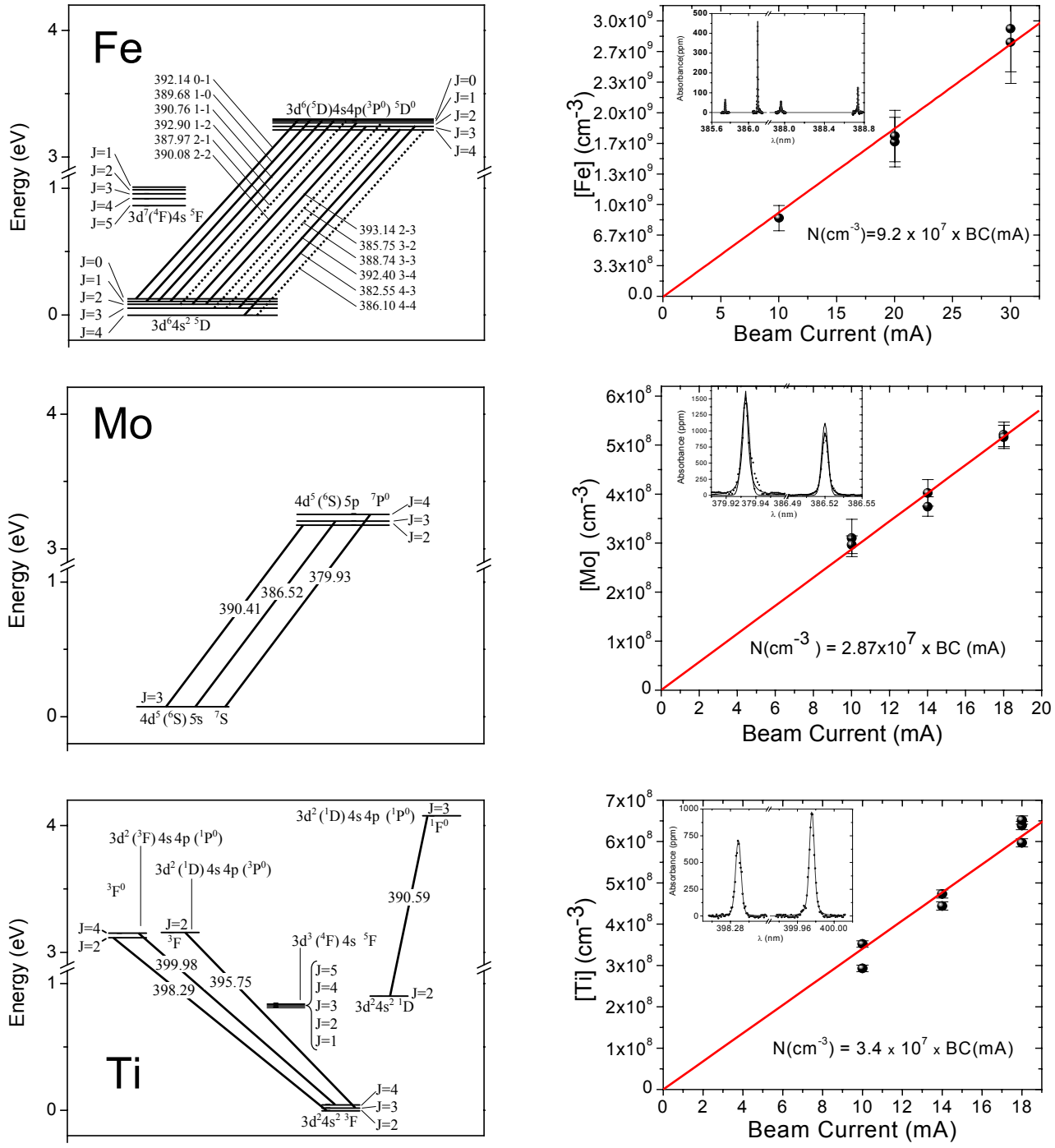

Figure 3. Left: Partial energy level diagrams for Al, Fe, Ti, Mo. All energy levels below 1 eV are included. Right: Number density versus beam current for Al, Fe, Ti, Mo. Insets show individual CRDS spectra.

B. Validation and Detection Limits of Bench-Top System

Figure 3 shows that the measured number densities are proportional to beam current, which is as expected. While the beam current data is useful for trend validation it does not provide absolute validation. As another means of validation we have developed a simple sputter model to numerically predict the path-integrated number densities. The simplified sputtering model assumes a (diffuse) cosine-distribution for the differential sputter yield and uses the

experimental beam current density (~30% uncertainty due to beam divergence and scattering effects) and target/optical-axis geometry (described in Section III). The model uses a finite element approach for both the target and optical axis, and computes the contribution of sputtered particles from each target element to each element along the optical axis. Summing the number densities along the extent of the optical axis then yields the path-integrated number density. The results are insensitive to the grid size. For 750 eV ions we use total sputter yields of 0.7+/-0.2 for titanium, 0.9+/-0.3 for molybdenum, 1.1+/-0.1 for aluminum, and 1.1+/-0.1 for iron[14]. For each material, the model requires the angular profile of (the average inverse) ejected velocity of the sputtered particles, which we have found using the TRIM sputtering simulation software (~20% uncertainty). We implicitly assume that the velocity simulations apply to all energy levels probed, an assumption consistent with LIF measurements of velocity fields (see Ref. 15 and references therein). For beam currents of 18 mA (30 mA for Fe), the path-integrated number densities found from the sputter code and measured by CRDS are given in Table 1.

We find good agreement (within error bars) between model and experiment for titanium, iron, and aluminum with the model being slightly higher than experiment in each case. For these species, the model over-prediction is attributed primarily to divergence and scattering of the ion beam, which makes the actual current density (and total current on the target) lower than the modeled value (which assumes no divergence). A secondary contribution to the discrepancy may be due a (relatively small) fraction of the sputtered particles having anomalously high energies (i.e. energy levels outside the ground state multiplet, see Section VI), since such particles are not measured by our CRDS scheme but would be included in the sputter yields. The larger molybdenum discrepancy (factor of ~1.5-3) is likely due to the above factors as well as an incorrect modeled sputter yield, related to details of the Mo sample preparation. The samples used in our experiments were obtained from 0.51 mm thick molybdenum sheets that were arc-cast and cross-rolled and tested as received (without polishing). Variation of sputter yield with the surface finish is to be expected and is also observed in quartz crystal microbalance (QCM) weight deposition measurements performed in our lab[16]. We take the overall positive agreement between our experimental and modeled results as validation of the CRDS sputter measurement technique.

Line Density:	Ti	Mo	Fe	Al
CRDS (cm^{-2})	$5.1\pm0.5 \times 10^{9}$	$4.1\pm0.4 \times 10^{9}$	$2.3\pm0.2 \times 10^{10}$	$7.2\pm0.7 \times 10^{9}$
Model (cm^{-2})	$8.7\pm4.0 \times 10^{9}$	$13\pm6.4 \times 10^{9}$	$2.6\pm1.0 \times 10^{10}$	$12\pm4.4 \times 10^{10}$

Table 1. Comparison of path-integrated number densities found from CRDS and sputter model.

The noise levels of our CRDS detection system can be used to estimate the minimum detectable (path-integrated) number density for each species studied. For most of our measurements the noise in the absorbance baseline is ~2 ppm (for measurement times of about 30 seconds). Our noise is primarily due to the relatively poor and unstable spatial mode of the OPO probe laser beam (the doubled-idler), which cause fluctuations in the ring-down signals. Pulsed CRDS experiments using dye lasers (with higher quality beam profiles) can have absorbance noise of ~0.1 ppm. Table 2 gives experimental detection limits for path-integrated number density for noise levels (in absorbance) of 2 and 0.1 ppm. In our experiments the path length is approximately 8 cm, so that corresponding number densities can be found accordingly. The detection limits of Table 2 (even for 2 ppm noise) are very adequate from the point of view of electric propulsion studies, where typical number densities of sputtered particles (from eroded components) are $\sim10^{8}$ cm^{-3} and path lengths are order 10 cm, so that typical path-integrated number densities are $\sim10^{9}$ cm^{-2}.

Noise Level	Ti (cm^{-2})	Mo (cm^{-2})	Fe (cm^{-2})	Al (cm^{-2})
2 ppm	$\sim7 \times 10^{7}$	$\sim6 \times 10^{6}$	$\sim6 \times 10^{7}$	$\sim6 \times 10^{6}$
0.1 ppm	$\sim4 \times 10^{6}$	$\sim3 \times 10^{5}$	$\sim3 \times 10^{6}$	$\sim3 \times 10^{5}$

Table 2. Minimum detectable path-integrated number densities by CRDS.

V. Velocity Measurements

Several laser techniques may be used for non-intrusive velocity measurements including filtered Rayleigh scattering (FRS), laser induced fluorescence (LIF), and laser absorption. In each case, the laser probes individual atoms (or molecules) within the flow field, and velocity information is found from Doppler shifts. For each of these techniques, a frequency reference measurement (e.g. from a stationary scatterer or absorber) is generally required. Here, we discuss our recently developed use CRDS to determine bulk velocity. Past work by other researchers has used CRDS for time-of-flight velocity measurements with pulsed sources, but our approach is based on Doppler shifts and is thus more generally applicable. A drawback of using CRDS for such studies is the path-integrated nature of the technique which limits its use in spatially varying flows. On the other hand, the use of CRDS for such measurements can provide complementary validation to other measurements (e.g. by LIF) and provides the possibility of simultaneous number density and velocity measurements. Further, the CRDS velocity measurements often can be performed without requiring an external frequency reference.

The absorptive nature of CRDS means that it can be used to measure bulk velocity from Doppler shifts associated with the velocity component(s) parallel to the optical axis. Because the laser beam propagates back-and-forth within the cavity, the light absorption for a moving particle is Doppler shifted *both* up- and down- in frequency. If the Doppler shift is large compared to the absorption linewidth, then the measured absorption feature is split into two peaks, and the peak separation provides a direct measure of velocity (see Fig.4). The relative laser frequency (i.e. separation of the peaks) must be known; however, in contrast to LIF, conventional absorption, or FRS, the absolute frequency is not required. Thus, application of CRDS velocimetry has the practical advantage of not requiring a precise frequency.

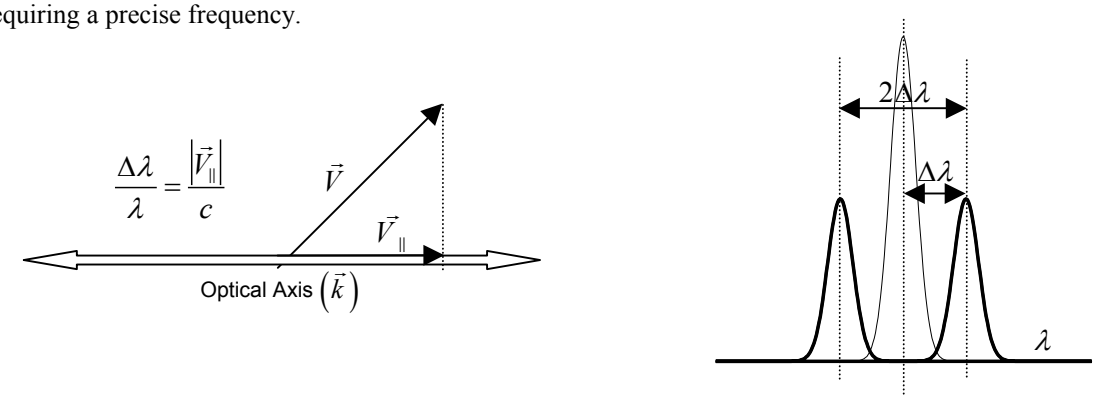

Figure 4. Left: Schematic of velocity vector, CRDS optical axis (wave vector points both directions), and velocity vector parallel to optical axis. Right: Measured CRDS lineshape (thick line) has both up- and down-shifted peaks. The separation of the shifted peaks, $2\Delta\lambda$, gives the parallel velocity component. The unshifted lineshape is shown with a thin line.

Details of the required expressions for the Doppler shifted lineshape $S(\nu)$ may be found in Ref. 8. Several laser techniques (especially LIF) may be used for velocity measurements based on Doppler shifts. We consider low-pressure (collisionless) free-molecular environments where the sputtered particles do not follow Maxwell-Boltzmann (MB) distributions, but rather have velocity profiles dictated by the sputtering conditions. The absorptive nature of CRDS means that bulk velocity (parallel to the optical axis) causes Doppler shifts. Because the laser beam propagates back-and-forth within the cavity, the light absorption for a moving particle is Doppler shifted *both* up- and down- in frequency. Thus, a measured absorption feature is split into two peaks, and the peak separation ($2\Delta\lambda$) provides a direct measure of velocity ($V=c\Delta\lambda/\lambda_0$). We assume linear cavity and a (spatially-dependent) number-density velocity distribution $n(\vec{V})$. The contribution to the Doppler lineshape from a given location along the optical-axis is:

$$S_x(\nu) \propto \left[n\left(V_{\parallel}\right) + n\left(-V_{\parallel}\right) \right] \tag{4}$$

where $V_{\parallel}$ is the velocity component of $\vec{V}$ parallel to the optical (x) axis, and the distribution of velocities $n(\vec{V})$ is expressed as a distribution of the form $n(V_{\parallel})$. Expression (4) should be integrated along the optical axis to find the overall Doppler lineshape $S(\nu)$. A similar expression results in LIF or conventional absorption, but only with a single term corresponding to a single peak.

We demonstrate the approach for sputtered atoms using the bench-top setup described above. The sputtered atoms are in a collisionless free-molecular regime (Knudsen number << 1). The velocities of the sputtered particles follow Thompson distributions (not MB) as predicted by linear-cascade theory. At these conditions, the only significant contributions to the measured lineshape are the Doppler shifted lineshape and the laser lineshape. We first consider a unidirectional velocity distribution which is achieved by affixing a honeycomb-like structure (HCS) normally onto the target. The HCS acts as a directional filter allowing only particles ejected normal to the target (±~20°) to reach the measurement volume. The optical axis is oriented at 45° to the surface normal. If the velocity distribution were sharply peaked, then $S(\nu)$ would be composed of two sharp peaks; however, the velocities of the sputtered atoms follow a distribution which smears the peaks. We assume a Thompson distribution of the form[18]:

$$n(V) \propto \frac{V^3}{\left(V^2 + V_b^2\right)^{n+1}}; \quad V_b = \sqrt{\frac{2E_b}{M}} \tag{5}$$

where E_b is the binding energy, M is the molar mass of the target material, and the exponent n is taken as 2 (for which the distribution is peaked at $V=V_b$). Fig. 5 shows split peaks in the measured lineshape (for Mo and Al targets, beam current of 60 mA, and beam voltage of 900 V). We fit the data assuming a Thompson distribution with V_b as a free (fit) parameter. The fit includes convolution with the laser lineshape (Lorentzian with FWHM=0.002 nm. We find the best fits for V_b=3500 m/s for Mo and V_b=4900 m/s for Al, which are in good agreement with calculated values of V_b=3700 m/s for Mo (E_b=6.82 eV) and V_b=4900 m/s for Al (E_b=3.36 eV). Our measurements are also validated by TRIM simulations which predict velocity profiles that are well fit by Thompson distributions with n=2 and the calculated V_b values. In principle, the data could be fit to obtain the full velocity distribution. If a similar experiment were performed with absorption or LIF, a single peak would be detected.

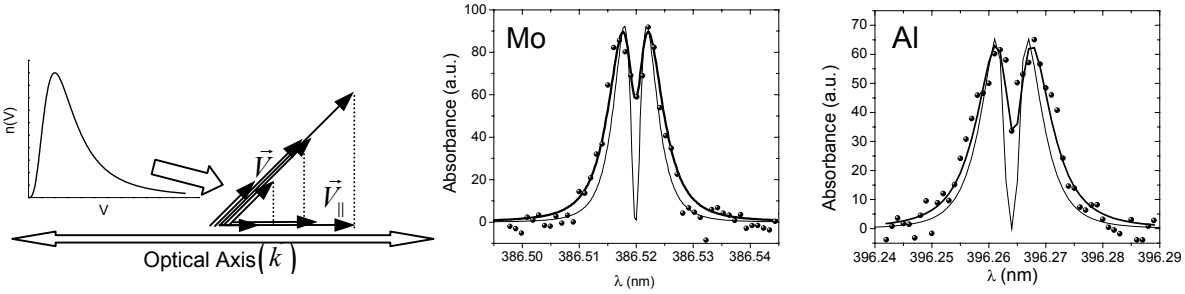

Figure 5. Left: Schematic representation of CRDS optical axis with multiple unidirectional velocity vectors oriented at 45°, and projections on optical axis. Middle/Right: Velocity measurements for Mo and Al. Symbols - measured lineshape; Thick line – model fit; Thin line – model fit without laser convolution.

We also consider a more complex but more realistic velocity field with sputtered particles ejected from the target in all directions, and the optical-axis perpendicular to the target surface normal. The overall Doppler lineshape is formed from a continuum of peaks due to the different velocity directions and amplitudes, resulting in a single broadened peak (similar but not the same as for a MB distribution). Fig. 6 shows CRDS data for sputtered Mo for a beam current of 18 mA and beam voltage of 750 eV. Computationally, we treat the target (8 cm parallel to the optical axis x 2.5 cm) as a series of finite elements. The differential sputter yield $y(\alpha)$ from each site is assumed to have a diffuse shape, i.e. $y(\alpha) \propto \cos(\alpha)$ where α is the ejection angle relative to the normal. We assume $n(V)$ is independent of α. We again fit the data using V_b as a free parameter, and find V_b=3300 m/s (uncertainty ~5%). The discrepancy with the expected value of 3700 m/s is thought to be primarily due to non-diffuse differential sputter yields, and/or velocity profiles having slight variation with the ejection angle α[19]. Even in the case of a relatively complex velocity field we are able to infer velocity information from the Doppler shifted lineshape.

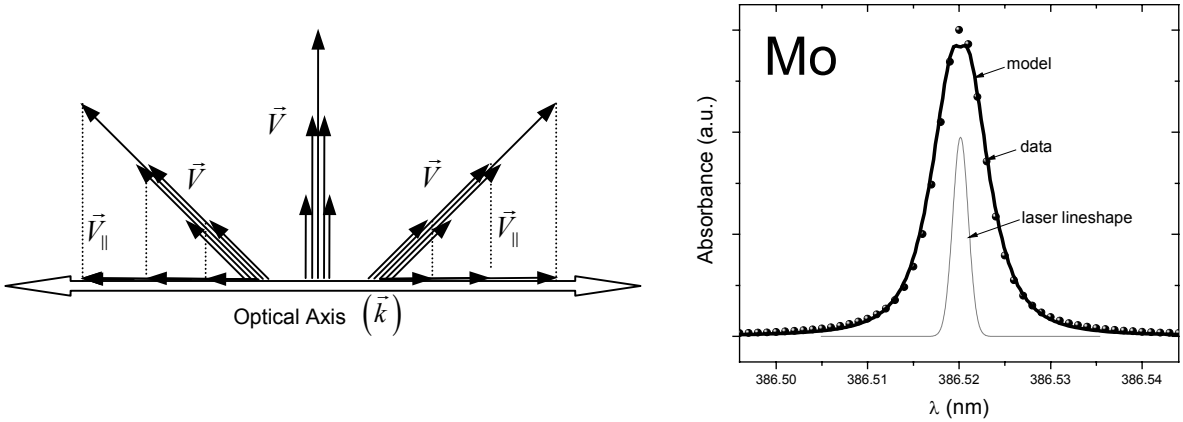

Figure 6. Left: Schematic representation of CRDS optical axis with multiple velocity vectors of differing directions and magnitudes, and projections on the optical axis. Right: Velocity measurement for Mo.

VI. Electronic Excitation of Sputtered Particles

The distribution (partitioning) of population over the available excited state energy levels of sputtered particles is both of theoretical interest (to model and understand the physical sputtering process) and of practical interest (to enable the conversion of measured populations from a subset of energy levels to the overall species population). In our past work we have studied the population distributions for iron, aluminum and titanium[7]. Here, we briefly review past findings (from our studies and those of other researchers) and then show results from dysprosium showing "anomalous" population distributions and the associated species specific velocities.

Past research has generally employed LIF as a diagnostic to study the populations of excited electronic states of sputtered particles[2,15,20]. These LIF studies generally found that although there is little physical basis to consider the sputtered particles as being in thermodynamic equilibrium, the populations of the sub-levels of a given multiplet can generally be described with a single Boltzmann temperature (at least as a means of characterization). It was found that these Boltzmann temperatures were typically in the range 300-2000 K, and that the distributions within different multiplets tend to follow different Boltzmann temperatures[2, 20]. In comparing the overall populations of different multiplets, it was also found that the characteristic temperature was also of the same order, meaning that high-lying states are minimally populated (e.g. states at >~ 1 eV have fractional population <~10^{-3}). On the other hand, several recent studies have shown unexpectedly high ("anomalous") populations of certain highly excited states in the sputtering of silver[21] and iridium[22], which would correspond to a non-physical Boltzmann temperature above 10,000 K (and thus emphasize the problems of assuming Boltzmann statistics).

We have used CRDS to examine the populations of the fine structure sub-levels of the electronic ground state multiplet for several species[7]. Consistent with past LIF studies, we found that the population of the various fine structure levels within the ground state multiplet could be characterized with a Boltzmann distribution with temperatures in the range of 500-2000 K. An unexpected result was that for Ti and Fe, the characteristic Boltzmann temperature was found to increase with the incident ion energy (rising from about 1000 to 1500 K as the incident ion energy increased from 300 to 800 eV).

Here, we present results of population distributions amongst energy levels for sputtered dysprosium (Dy). Dy was selected for such studies owing to its large number of (accessible) electronic energy levels. We have measured absorbance spectra, populations, and velocities of seven (fine structure) electronic levels that arise from two different electronic configurations (see Fig. 7): $4f^{10}\ 6s^2$ ($^5I_8$ and $^5I_7$) and $4f^9 5d6s^2$ ($^7H_8$, $^7H_7$, $^7I_9$, $^7F_6$, and $^5G_6$). The level populations are found as in Section IV and are summarized in Fig. 7. The populations N_i (corrected for degeneracy) are given relative to the ground state as a function of excitation energy above the ground state. (A Boltzmann distribution of states would appear linear on such a plot.) The ground state corresponds to a $4f^{10}\ 6s^2$ outer shell electronic configuration and the other states correspond to $4f^9\ 5d^1\ 6s^2$ outer shell electronic configuration. Fig. 7 shows that within a single multiplet, the relative populations do decrease exponentially and can be described by a Boltzmann temperature (distribution). Fitting the data yields T_B=1425+/-100 K for the ground state $\{^5I_J\}$, and T_B= 1000+/-50 K for the first excited multiplet $\{^7H_J\}$. On the other hand, comparing the multiplets to one another yields rather different (characteristic) Boltzmann temperatures. The relative population of the $^7H_8$ level (E=0.93 eV) as compared to the ground state corresponds to a (non physical) effective Boltzmann temperature of 4850+/-150 K. This "anomalous" distribution is similar to that found in other recent studies[21, 23]. The relatively high population of the excited states (e.g. E=0.938 eV has 10% of the population of the ground state) may be explainable by the

resonant electron transfer model (RET) [26-30, 22]. In the RET model the metal is considered as a lattice of positive ions in a gas of delocalized electrons. When an energetic projectile (incident ion) triggers a collision cascade at the metal surface, the sputtered particles are neutralized by picking up an electron. The RET model considers the energy level populations (of the sputtered atoms) on the basis of the overlap (coupling) of the energy levels of electrons of the solid with the energy levels of the ejected atoms, as well as the overlap of the corresponding wave functions. The model predicts that energy levels with energies relative to the ground state of less than the difference between the ionization potential and work function of the solid can have significant populations. For dysprosium, the ionization potential is 5.94 eV and the work function is 2.89 eV, so that the RET predicts that levels with excitation energies up to ~3 eV can be populated (since they lie below the Fermi level). Our results may be consistent with such an interpretation. An interesting observation from the data is that there are no apparent negative temperatures (i.e. population inversions).

We have also examined the (level-specific) velocities using the full multi-directional profiles as discussed in Section V. Results of the velocity measurements, i.e. the fitted values of V_b, are illustrated in Fig. 8. The left of Fig. 8 shows measured profiles for energy levels of 0 eV and 1.97 eV. Also included are lineshape fits using the best-fit velocities of V_b=1450 m/s and V_b=3450 m/s respectively. (The broader profile for the 1.97 eV case is a clear qualitative indication of its larger velocity.) The right of Fig. 8 shows the fitted velocities plotted versus the level energies. The results of Fig. 8 are qualitatively consistent with those of other researchers[2, 20]. We find that the velocities of different levels within a given multiplet (e.g. $^5I_8$ and $^5I_7$ within the lowest multiplet, and $^7H_8$ and $^7H_7$ within the first excited multiplet) are uniform, and that as the energy of the multiplet increases the velocity increases. The latter observation has been explained on the basis that the excited states form more quickly, and thus are more likely to be formed from atoms leaving the surface with higher velocities.

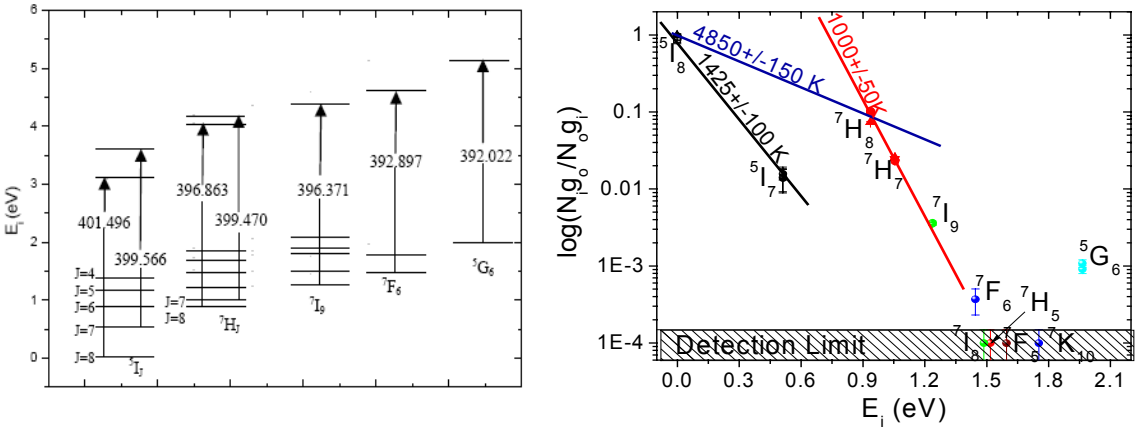

Figure 7. Left: Partial energy level diagram. Right: The relative population of different atomic states of Dy produced by 750eV Ar^+ ion bombardment.

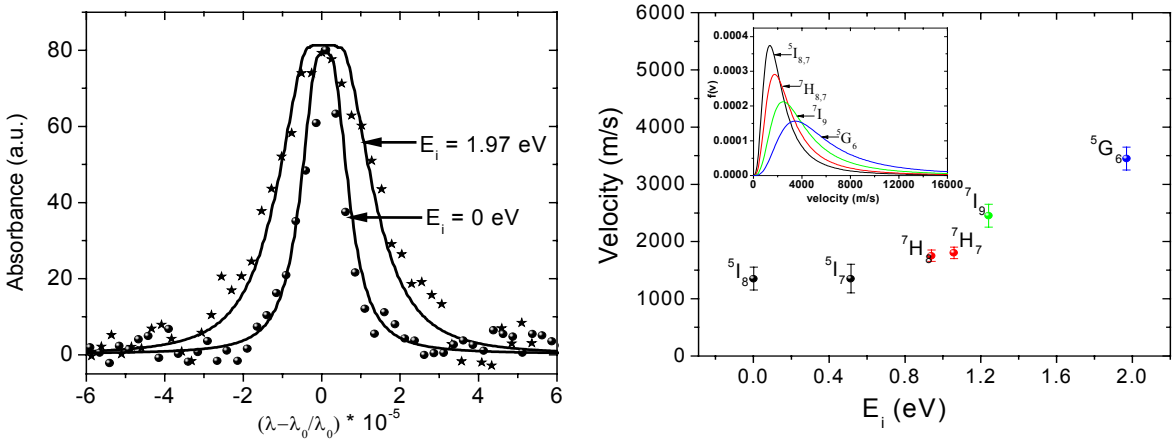

Figure 8. Left: Measured profiles and fits for energy levels of 0 eV ($^5I_8$) and 1.97 eV ($^5G_6$). Right: Fitted velocities (V_b) for several energy levels. Inset shows the profiles corresponding to the fitted V_b values.

VII. Summary

We have demonstrated CRDS as a versatile tool for quantitative diagnostics of sputter erosion processes, including measurements of sputtered particle number density and velocity. We have presented number density measurements of several metal species including validation with a simple sputter model. For EP applications one generally hopes to measure the flux of sputtered particles (for erosion estimates, sputter yield determinations etc.), which requires knowledge of both particle number density and particle velocity. In this work, we have also demonstrated the possibility of using CRDS for velocity measurement. The CRDS velocimetry technique is well suited to measurements in low-pressure collisionless environments since the overall lineshape is dominated by the Doppler shifts. We recognize the limitations posed by the path-integrated nature of CRDS in terms of implementing it for velocity measurements; however, in certain geometries such implementations are possible and afford the advantages of not requiring an external frequency reference, and the possibility of simultaneous number density and velocity measurements. In more complex measurement environments, the needed velocity information can be derived from laser induced fluorescence and/or modeling. We have also shown the use of CRDS (via both number density and velocity measurements) for studying the distribution of excited states of sputtered particles. Such studies are of both basic and applied interest (e.g. in EP one needs knowledge of such distributions to relate the population of a single measured state to the overall species populations). For dysprosium we have observed anomalously high populations of excited states that cannot be reasonably described with Boltzmann statistics.

Owing to its highly sensitive and highly quantifiable nature, CRDS has the potential to provide a powerful sputtering gauge that may be superior to other available optical and non-optical sputter diagnostic techniques. Its quantitative and linear nature (that does not require external calibration) provides a clear advantage over LIF for number density measurements. Further, the simple nature of CRDS (as compared to say surface layer activation) makes it very amenable to *in situ* applications, for example real time studies of device erosion rates, as a function of device operating conditions. Finally, the spectroscopic nature of CRDS makes it appropriate for species-specific studies of the sputtering of multi-component mixtures; for example, studying how the boron sputters from a boron nitride insulator. We are currently undertaking such studies to address spacecraft contamination by condensed sputter products.

Acknowledgments

The research was funded by Air Force Research Laboratory, Edwards Air Force Base, and NASA's Exploration Systems Missions Directorate.

References

[1]Kolasinski, R.D. and Polk, J.E., "Characterization of cathode keeper wear by surface layer activation," AIAA Paper No. 2003-5144, in 39th AIAA Joint Propulsion Conference, Huntsville, AL, 2003.

[2]Bay, H.L., "Laser induced fluorescence as a technique for investigations of sputtering phenomena," Nuclear Instruments and Methods, Vol.18, p. 430-445, 1987.

[3]Pellin, M.J., Young, C.E., Mendelsohn, M.H., Gruen, D.M. , Wright, R.B., and Dewald, A.B., "Oxygen and titanium sputtering yields as determined by laser fluorescence and auger electron spectroscopy for monolayer oxygen coverage of polycrystalline Ti," Journal of Nuclear Materials, 111 & 112, p. 738-743, 1982.

[4]Busch, K.W., and Busch, M.A., "Cavity-Ringdown Spectroscopy," ACS Symposium Series, Vol. 720, 1999.

[5]Berden, G., Peeters, R., and G. Meijer, "Cavity Ring-Down Spectroscopy: Experimental Schemes and Applications," International Reviews in Physical Chemistry, Vol.19, No.4, p. 565-607, 2000.

[6]Surla, V., Wilbur, P.J., Johnson, M., Williams, J.D., Yalin, A.P., "Sputter erosion measurements of titanium and molybdenum by cavity ring-down spectroscopy," Review of Scientific Instruments, Vol.75, No.9, p. 3025-3030, 2004.

[7]Yalin, A.P., Surla, V., Butweiller, M., Williams, J.D., "Detection of Sputtered Metals using Cavity Ring-Down Spectroscopy," Applied Optics (to be published).

[8]Yalin, A.P., Surla, V., "Velocity Measurements by Cavity Ring-Down Spectroscopy," Optics Letters (to be published).

[9]Zalicki, P. and Zare, R.N., "Cavity ring-down spectroscopy for quantitative absorption measurements," Journal of Chemical Physics, Vol. 102, No.7, p. 2708-17, 1995.

[10]Yalin, A.P., and Zare, R.N., "Effect of Laser Lineshape on the Quantitative Analysis of Cavity Ring-Down Signals," Laser Physics, Vol.12, No.8, p. 1065-1072, 2002.

[11]Hudson, W.R. and Banks, B.A., "An 8-cm electron bombardment thruster for auxiliary propulsion," AIAA Paper No. 73-1131, in 10th AIAA Electric Propulsion Conference, Lake Tahoe, NV, 1973.

[12]Spuler, S. and Linne, M., "Numerical analysis of beam propagation in pulsed cavity ring-down spectroscopy," Applied Optics, Vol.41, No.15, p. 2858-2868, 2002.

[13]NIST, data base available in monographs or URL: http://physics.nist.gov/PhysRefData/ASD/index.html.

[14]Yamamura, Y. and Tawara, H., "Energy Dependence of Ion-Induced Sputtering Yields from Monatomic Solids at Normal Incidence," Atomic Data and Nuclear Data Tables, Vol.62, No.2, p. 149-253, 1996.
[15]Betz, G. and Wien, K.," Review: Energy and angular distributions of sputtered particles," International Journal of Mass Spectrometry and Ion Processes, Vol.140, p. 1-110, 1994.
[16]Williams, J.D., Gardner, M.M., Johnson, M., and Wilbur, P.J., "Xenon Sputter Yield Measurements for Ion Thruster Materials," Paper No.2003-0130, in 28th International Electric Propulsion Conference, Toulouse, France, 2003.
[17]Bay, H.L., Schweer, B., Bogen, P., and Hintz, E., "Investigation of light-ion sputtering of titanium using laser-induced fluorescence," Journal of Nuclear Materials, Vol.111 & 112, p. 732-737, 1982.
[18]Pellin, M.J., R.B. Wright, and D.M. Gruen, "Laser fluorescence spectroscopy of sputtered zirconium atoms," Journal of Chemical Physics, Vol.74, No.11, p. 6448-6457, 1981.
[19]Goehlich, A., "Investigation of time-of-flight and energy distributions of atoms and molecules sputtered from oxygen-covered metal surfaces by laser techniques," Applied Physics A, Vol.72, p. 523-529, 2001.
[20]Betz, G., "Electronic excitation in sputtered atoms and the oxygen effect," Nuclear Instruments and Methods in Physics Research Section B, Vol.27, p. 104-118, 1987.
[21]Staudt, C., Wucher, A., Bastiaansen, J., Philipsen, V., Vandeweert, E., Lievens, P., Silverans, R.E., and Sroubek, Z., "Sputtering of Ag atoms into metastable excited states," Physical Review B, Vol.66, p. 085415 1-12, 2002.
[22]Bastiaansen, J., Philipsen, V., Lievens, P., Silverans, R.E., and Vandeweert, E., "Influence of atomic structure on the quantum state of sputtered Ir atoms," Physical Review A, Vol.70, 2004.
[23]He, C., Postawa, Z., Rosencrance, S., Chattterjee, R., Garrison, B.J., and Winograd, N., "Band Structure Effects in Ejection of Ni Atoms in Fine Structure States," Physical Review Letters, Vol.75, No.21, p. 3950, 1995.
[24]Young, C.E., Calaway, W.F., Pellin, M.J., and Gruen, D.M., "Velocity and electronic state distributions of sputtered Fe atoms by laser-induced fluorescence spectroscopy," Journal of Vacuum Science technology A, Vol.2, No.2, p. 693-697, 1984.
[25]Dullni, E., "Laser fluorescence measurements of the flux density of titanium sputtered from an oxygen covered surface," Applied Physics A, Vol.38, p. 131-138, 1985.
[26]Vandeweert, E., Lievens, P., Philipsen, V., Bastiaansen, J., and Silverans, R.E., "Measurements of population partitions and state-selected flight -time distributions of keV ion-beam-sputtered metastable atoms," Physical Review B, Vol.64, 2001.
[27]Vandeweert, E., J.B., Philipsen, V., Lievens, P., and Silverans, R.E., "Resonant electron transfer during ion-beam sputtering of metals studied by double-resonant laser ionization," Nuclear Instruments and Methods in Physics Research Section B, Vol.164-165, p. 795-802, 2000.
[28]Bastiaansen, J., Vervaecke, F., Vandeweert, E., Lievens, P., and Silverans, R.E., "Electronic processes during the sputtering of atoms from metallic surfaces studied by resonance laser ionization spectroscopy," Spectrochemica Acta Part B, Vol.58, p. 1147-1154, 2003.
[29]Bastiaansen, J., Philipsen, V., Vervaecke, F., Vandeweert, E., Lievens, P., and Silverans, R.E., "Velocity dependent electron transfer during emission of ion-beam sputtered Cu atoms," Physical Review B, Vol.68, 2003.
[30]Bastiaansen, J., Vervaecke, F., Vandeweert, E., Lievens, P., and Silverans, R.E., "Modeling the multichannel electron transfer during the sputtering of Co atoms," Nuclear Instruments and Methods in Physics Research Section B, Vol.203, p. 158-163, 2003.